# Study of the Evaporation of Colloidal Suspension Droplets with the Quartz Crystal Microbalance

**ARTICLE** *in* LANGMUIR · AUGUST 2008

Impact Factor: 4.46 · DOI: 10.1021/la800661g · Source: PubMed



**4 AUTHORS**, INCLUDING:

Pin Lu
Hefei University of Technology
**82** PUBLICATIONS **1,614** CITATIONS
SEE PROFILE

Hp Lee
National University of Singapore
**321** PUBLICATIONS **5,239** CITATIONS
SEE PROFILE

# Study of the Evaporation of Colloidal Suspension Droplets with the Quartz Crystal Microbalance

Han Zhuang,*[,†] Pin Lu,[‡,§] Siak Piang Lim,[†] and Heow Pueh Lee[†,‡]

*Department of Mechanical Engineering, National University of Singapore, 1 Engineering Drive 2, 117576 Singapore, Institute of High Performance Computing, 1 Science Park Road, #01-01 Capricorn Science Park II, 117528 Singapore, and Department of Modern Mechanics, University of Science and Technology of China, Hefei, Anhui 230027, People's Republic of China*

*Received March 3, 2008. Revised Manuscript Received May 20, 2008*

In this Article, we report the application of the quartz crystal microbalance (QCM) to study the evaporation of colloidal suspension droplets. Droplets of alumina particle suspensions with varying particle size and solid concentration have been investigated. Characteristic responses of the resonance frequency of the QCM associated with the different evaporation stages have been established. Quantitative analysis of the experimental results has been performed by the proposed QCM models. An interesting finding is that frequency increase after complete drying has been observed in some cases. Interpretation of the frequency increase has been developed in terms of the contact stiffness. The possible physical mechanisms are also discussed and quantified in terms of various interparticle forces.

## Introduction

Sessile droplet evaporation on a surface has been well documented since Maxwell in 1877 addressed the evaporation of a spherical droplet and also has been studied using the quartz crystal microbalance (QCM),[1] which has its origin in the pioneering work of Sauerbrey. Recent work by Joyce et al.[2] studied the evaporation of sessile droplets of homologous series of alcohols on the crystal surface. It showed that the extreme modes of droplet evaporation, associated with constant contact area and constant contact angle, could be deduced from the frequency responses of the QCM. McKenna et al.[3] studied the evaporation of droplets of water with simultaneous QCM measurements and microscopy. It showed that the evaporation processes including the pinned contact area and the retreating contact line stages could be characterized by the resonant frequency changes, which were related to the droplet placement on the electrode. It also observed noticeable discontinuities in the responses caused by the compression wave generations for noncentrally located droplets. Besides the liquid droplet measurements, the QCM has been extensively used to detect the properties of material on its surface. During the last decades, the QCM has been demonstrated to be a promising tool to probe interfacial phenomena including gas adsorption kinetics,[4,5] adsorption/desorption in liquids,[6,7] and wetting behaviors of liquid droplets.[8,9] Further work has focused on thin films,[10,11] adhesion of polymers,[12] and in biotechnology the cell and protein adhesion kinetics.[13]

Recently, the drying of colloidal suspensions has been a subject of growing interest and has found applications in diverse industries such as biochemical, agricultural, food, pharmaceutical, printing, and mineral industries.[14] Parisse et al.[15] studied the morphological changes of droplets of concentrated colloidal suspensions under drying on the flat substrate. They showed that the droplet profile during the evaporation could be interpreted using a renormalization procedure and that a simplified model could be used to describe the renormalized film thickness. Dalmaz et al.[16] addressed a computational single-droplet model to simulate the evaporation of colloidal silica−water suspension and skimmed milk. They found that the model could be applied to investigate the effects of main drying parameters such as the droplet size and solid concentration. However, there have been only a few studies on the responses of the QCM in contact with aqueous suspension droplets. Bell et al.[17] investigated the change in the frequency of the QCM with varying solid concentration of the colloidal suspensions. They found that, within the uncertainty of the experiments, the presence of the colloidal particles had no influence on the frequency responses of the QCM. Lec et al.[18] studied the sedimentation processes of colloidal suspensions using the QCM frequency measurements. Their results showed that the QCM could be applied to monitor and analyze the sedimentation processes of colloidal suspensions in real-time mode. However, the drying of colloidal suspensions has seldom

* Corresponding author. E-mail: g0402941@nus.edu.sg.
† National University of Singapore.
‡ Institute of High Performance Computing.
§ University of Science and Technology of China.

(1) Fuchs, N. A. *Evaporation of Droplet Growth in Gaseous Media*; Pergamon Press: London, 1959.
(2) Joyce, M. J.; Todaro, P.; Penfold, P.; Port, S. N.; May, J. A. W.; Barnes, C.; Peyton, A. J. *Langmuir* **2000**, *16*, 4024.
(3) McKenna, L.; Newton, M. I.; McHale, G.; Lucklum, R.; Schroeder, J. *J. Appl. Phys.* **2001**, *89*, 676.
(4) Ward, M. D.; Buttry, D. A. *Science* **1990**, *249*, 1000.
(5) Ali, Z.; Thomas, C. L. P.; Marshall, G. B.; Alder, J. F. *Analyst* **1992**, *117*, 899.
(6) Weerawardena, A.; Drummond, C. J.; Caruso, F.; McCormick, M. *Langmuir* **1998**, *14*, 575.
(7) Schumacher, R. *Angew. Chem.* **1990**, *29*, 329.
(8) Lin, Z.; Hill, R. M.; Davis, H. T.; Ward, M. D. *Langmuir* **1994**, *10*, 4060.
(9) Zhuang, H.; Lu, P.; Lim, S. P.; Lee, H. P. *Langmuir* **2007**, *23*, 7392.
(10) Forrest, J. A.; Dalnoki-Veress, K.; Dutcher, J. R. *Phys. Rev. E* **1998**, *58*, 6109.
(11) Wang, J.; Ward, M. D.; Ebersole, R. C.; Foss, R. P. *Anal. Chem.* **1993**, *65*, 2553.
(12) Brass, D. A.; Shull, K. R. *Langmuir* **2006**, *22*, 9225.
(13) Stadler, H.; Mondon, M.; Zeigler, C. *Anal. Bioanal. Chem.* **2003**, *375*, 53.
(14) Brinker, C. J.; Scherer, G. W. *Sol−Gel Science: The Physics and the Chemistry of Sol−Gel Processing*; Academic Press: San Diego, 1990; Chapter 1.
(15) Parisse, F.; Allain, C. *Langmuir* **1997**, *13*, 3598.
(16) Dalmaz, N.; Ozbelge, H. O.; Eraslan, A. N.; Uludag, Y. *Drying Technol.* **2007**, *25*, 391.
(17) Bell, J.; Köhler, T.; Woermann, D. *Ber. Bunsen-Ges. Phys. Chem.* **1997**, *101*, 879.
(18) Lec, R. M.; Sorial, J. *IEEE Int. Freq. Contr. Symp. PDA Exhib.* **2001**, 838.

10.1021/la800661g CCC: $40.75 
Published on Web 07/11/2008

been studied by using the QCM. Although Serizawa et al.[19] studied the electrostatic adsorption of the polystyrene nanoparticles onto the modified QCM surface, their experiments were done ex situ after complete drying and did not reflect the drying kinetics. In addition, Pham et al.[20] investigated the kinetics of the evaporation of pure water as well as latex and clay particle suspensions using the QCM. They found that the QCM responses exhibited the dependency on the particle size and that the different evaporation stages could be described by the QCM results.

In this Article, we extend the work by Pham et al. by presenting the experiment results for the evaporation of alumina particle suspension droplets located on the QCM surface. This process was encountered when we sorted alumina powders to be used for ceramic tool sintering.[21] Droplets of the suspensions with different particle size and solid concentration are used to study the effects of the solid phase adsorption onto the QCM surface during the evaporation. Quantitative analysis of the evaporation phenomena is presented using the QCM models proposed in this Article. Moreover, positive frequency changes after complete drying are observed for some suspensions. Physical mechanisms for these positive frequency changes are discussed and quantified in terms of interactions between particles such as the van der Waal force and the capillary force.

## Theory

**A. Review of QCM Models for Loading with Solid Particles.** The AT-cut quartz crystal with circular electrodes on both sides can be electrically excited in the thickness-shear mode. The small-load approximation is commonly used to model the responses of the QCM.[22] Herein, the small-load approximation means that the frequency shift $\Delta f$ is small as compared to the resonant frequency $f_f$ ($\Delta f/f_f \ll 1$). The complex frequency shift $\Delta\tilde{f} = \Delta f + \Delta\Gamma$ then is

$$\frac{\Delta\tilde{f}}{f_f} = \frac{\Delta f + i\Delta\Gamma}{f_f} \approx \frac{i}{\pi Z_q} Z_L = \frac{i}{\pi Z_q}\frac{\sigma}{\dot{u}} \tag{1}$$

where $\Delta\Gamma$ is the change in half-band-half-width, and $Z_q = 8.8 \times 10^6$ kg m$^{-2}$ is the acoustic impedance of the quartz crystal. The load impedance $Z_L$ is the ratio of the stress $\sigma$ and the speed $\dot{u}$ at the crystal surface. The small-load approximation shows that $\Delta f$ and $\Delta\Gamma$ are proportional to the imaginary and the real part of the load impedance $Z_L$.

If the QCM electrode is partially covered by a material, recent work has demonstrated that the effect of the finite contact area on the resonant frequency can be manifested as a modification of the small-load approximation equation:[23]

$$\frac{\Delta f}{f_f} = \frac{i}{\pi Z_q} K_A \frac{A_C}{A_0} Z_L \tag{2}$$

where $A_C$ is the macroscopic contact area covered by the coated layer and $A_0$ is the active area of the quartz crystal herein referring to the area of the smaller electrode. It assumes that the radius of the macroscopic contact area between the crystal and the attached media is much larger than the shear wave decay length. The sensitivity factor $K_A$ accounts for the effects of the Gaussian radial amplitude distribution across the crystal surface:[3,8,23]

$$K_A \frac{A_C}{A_0} = 1 - \exp\left(-2\beta\frac{A_C}{A_0}\right) \tag{3}$$

where $\beta$ is a parameter defining the distribution of the amplitude dependence on $A_0$. $\beta$ was chosen to be 2 in the present analysis for simplicity.[8] In the full coverage case, we have $K_A = 1$, whereas for small contact coverage ($A_C/A_0 \ll 1$), the QCM response will be approximately twice as sensitive as the full coverage case where $K_A \approx 2$.[23]

Modeling the particles as solid spheres and assuming that they are rigidly attached to the crystal, the motions of the spheres are in phase with the motion of the crystal. We denote $m_S$ and $N_S$ as the mass and number of the spheres. The areal mass density is then defined as $m_f = m_S N_S/A_0$. Using the stress $\sigma = -\omega^2 m_f a$ ($a$ is the amplitude of the oscillatory displacement and $\omega$ is the angular frequency) and the speed $\dot{u} = i\omega a \exp(i\omega t)$, the frequency shift is given by:

$$\frac{\Delta f}{f_f} = \frac{i}{\pi Z_q} K_A \frac{A_C}{A_0} Z_L = \frac{i}{\pi Z_q} K_A \frac{A_C}{A_0}\frac{-\omega^2 m_f a \exp(i\omega t)}{i\omega a \exp(i\omega t)} = \frac{-\omega m_f}{\pi Z_q} K_A \frac{A_C}{A_0} \tag{4}$$

In the other limit, as inertia holds the spheres in place, only the contact stiffness will be detected.[24,25] We can use one spring with spring constant $\kappa_S$ to represent the effective contact stiffness detected by the QCM. The resulting frequency shift can also be given by the small-load approximation if the average stress is given by the restoring force of the spring multiplied the number density:

$$\frac{\Delta f}{f_f} = \frac{i}{\pi Z_q} K_A \frac{A_C}{A_0}\frac{\sigma}{\dot{u}} = \frac{i}{\pi Z_q} K_A \frac{A_C}{A_0}\frac{N_S}{A_0}\frac{\kappa_S u}{i\omega u} = \frac{1}{\pi Z_q} K_A \frac{A_C}{A_0^2}\frac{N_S \kappa_S}{\omega} \tag{5}$$

where $u = a \exp(i\omega t)$ is the oscillatory displacement. Equation 5 predicts a positive frequency shift proportional to the effective contact stiffness. Equation 5 can be extended to account for the spheres partially coupled to the lateral oscillation of the crystal, which is represented by a mass in series with a spring. If the spring constant is still labeled by $\kappa_S$, the load impedance then is:

$$Z_L = \frac{N_S}{A_0}(Z_{mass}^{-1} + Z_{spring}^{-1})^{-1} = \frac{N_S}{A_0}\left(\frac{1}{i\omega m_S} + \frac{i\omega}{\kappa_S}\right)^{-1} = \frac{N_S}{A_0} i\omega m_S \frac{1}{1 - \frac{\omega^2}{\omega_S^2}} \tag{6}$$

where $\omega_S = (\kappa_S/m_S)^{1/2}$ represents the angular resonant frequency of a solid sphere. Using the small-load approximation, the frequency shift can be found as:

$$\frac{\Delta f}{f_f} = \frac{i}{\pi Z_q} K_A \frac{A_C}{A_0} Z_L = \frac{-\omega m_S}{\pi Z_q} K_A \frac{A_C N_S}{A_0^2}\frac{1}{1 - \frac{\omega^2}{\omega_S^2}} \tag{7}$$

In the limits of $\omega_S \gg \omega$ and $\omega_S \ll \omega$, it recovers the mass loading model (eq 4) and the simple-spring model (eq 5), respectively.

(19) Serizawa, T.; Takeshita, H.; Akashi, M. *Langmuir* **1998**, *14*, 4088.
(20) Pham, N. T.; McHale, G.; Newton, M. I.; Carroll, B. J.; Rowan, S. M. *Langmuir* **2004**, *20*, 841.
(21) Lim, L. C.; Wong, P. M.; Ma, J. *J. Mater. Process. Tech.* **1997**, *67*, 137.
(22) Johannsmann, D.; Mathauer, K.; Wenger, G.; Knoll, W. *Phys. Rev. B* **1992**, *46*, 7808.
(23) Flanigan, C. M.; Desai, M.; Shull, K. R. *Langmuir* **2000**, *16*, 9825.
(24) Dybwad, G. L. *J. Appl. Phys.* **1985**, *58*, 2789.
(25) D'Amour, J. N.; Stålgren, J. J. R.; Kanazawa, K. K.; Frank, C. W.; Rodahl, M.; Johannsmann, D. *Phys. Rev. Lett.* **2006**, *96*, 058301.

The contact stiffness depends on interaction forces between the solid particles present on the QCM. The shear motion of the crystal could be affected by the contact stiffness, which comes from various sources of interaction forces such as van der Waals force, capillary force, friction force, electrostatic force, gravitational force, etc. There has been considerable advance in recent years in understanding the various interaction forces between solid particles with different techniques and instruments.[26] The van der Waals force plays a vital role as we consider phenomena involving the short-range interactions between the macroscopic particles. The van der Waals energy and van der Waals force between two identical spheres in air can be expressed as:[26]

$$W_{vdw}(D) = -\frac{A}{24}\frac{d_p}{D} \text{ and } F_{vdw}(D) = \frac{A}{24}\frac{d_p}{D^2} \quad (8)$$

where $D$ is the distance between the spheres, $d_p$ is the sphere's diameter, and $A$ is the Hamaker constant, about $(0.4-4) \times 10^{-19}$ J. Thus, the effective stiffness $k_S$ is:

$$k_S = -\frac{\partial F_{vdw}(D)}{\partial D} = \frac{A}{12}\frac{d_p}{D^3} \quad (9)$$

It indicates that the effective stiffness $k_S$ is dependent on the particle diameter $d_p$ as well as the inverse third order in interparticle distance $D$. It is also known that the mechanical and adhesion properties of granular matters are very sensitive to the presence of small quantities of water in ambient surrounding.[27,28] It has been found that the adhesion force between granular matters was drastically dependent on the ambient humidity as the condensation of water around the contact sites had a pronounced influence on the adhesion strength. This is commonly known as the sandcastle effect.[29,30] The capillary force due to the liquid bridge connecting two identical spheres can be modeled in the framework of classical capillary theory down to tiny radii of curvature $r$ of the liquid meniscus:[27]

$$F_{cal}(D) = \pi d_p \gamma_L \cos\theta(1 - D/2r) \quad (10)$$

where $\gamma_L$ is the surface tension of condensed liquid and $\theta$ is the contact angle, and $d_p$ is the radius of the spheres and $D$ is their distance. Thus, the effective stiffness $k_S$ will be:

$$k_S = -\frac{\partial F_{cal}(D)}{\partial D} = \frac{\pi d_p \gamma_L \cos\theta}{2r} \quad (11)$$

It indicates that the effective stiffness $k_S$ is dependent on the particle diameter $d_p$ as well as the inverse radii of curvature $r$ of the liquid meniscus. Also, the surface tension $\gamma_L$ and contact angle $\theta$ of the condensed liquid affect the effective stiffness $k_S$. Under certain conditions, such as proper grounding and discharging of the micro-/nanoparticles and the sensor, and the smooth surface of the sensor, other interaction forces, such as electrostatic force due to contact electrification or triboelectrification, frictional force, and gravitational force, are less important than the van der Waals force and the capillary force to account for the contact stiffness between the particles under our laboratory environment.

**B. Modified Model for QCM in Contact with Alumina Particles.** To further describe the experimental responses on loading with the alumina particles after drying various alumina suspension droplets, we apply the above models and include the interaction forces associated with the contact stiffness between the alumina particles. After the droplet of the alumina suspensions evaporates on the electrode of the crystal, it leaves behind a circular residual on the surface. If the amount of the alumina particles is less than a monolayer, it is expected that all alumina particles can be rigidly attached to the electrode surface. As a result, the frequency shift can be calculated by using the mass loading model, eq 4. It shows that when the added mass increases with suspension concentration, the resulting frequency shift decreases.

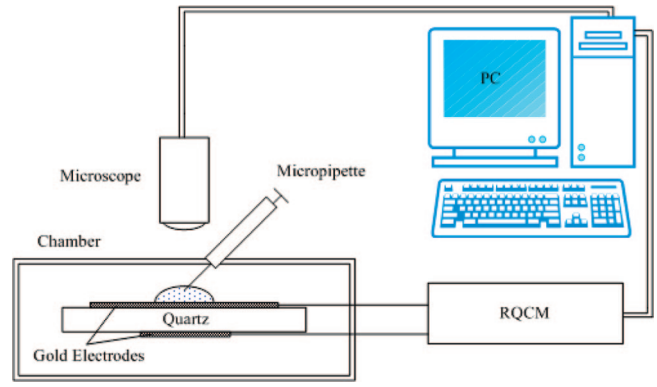


**Figure 1.** Schematic diagram of the experimental setup.

On the other hand, when the amount of the alumina particles exceeds the amount of the monolayer, the multilayer formation on the electrode is expected. It assumes that only the first layer is rigidly attached to the electrode surface whereas the second layer and higher layers are loosely bound with each other. Thus, the second layer and higher layers would not oscillate in phase with the underlying crystal. The interactions between the alumina particles could affect the response of the QCM. For the multilayer, we combine eqs 4 and 7:

$$\frac{\Delta f}{f_f} = \frac{-\omega m_S}{\pi Z_q} K_A \frac{A_C}{A_0^2}\left[N_M + (N_S - N_M)\Big/\left(1 - \frac{\omega^2}{\omega_S^2}\right)\right], \text{ at } N_S > N_M \quad (12)$$

where $N_M$ is the number of particles corresponding to a monolayer within the contact area. Equation 12 indicates that the resonant frequency of the QCM upon the multilayer deposition can either increase or decrease with increasing interparticle contact stiffness. It also shows that the mass effect could potentially be offset by adjusting the contact stiffness, which would result in a positive frequency shift.

Furthermore, we incorporate the equations of the van der Waals force (eq 9) and the capillary force (eq 11) into eq 12. For the van der Waals force, it will be:

$$\frac{\Delta f}{f_f} = \frac{-\omega m_S}{\pi Z_q} K_A \frac{A_C}{A_0^2}\left[N_M + (N_S - N_M)\Big/\left(1 - \frac{12\omega^2 m_S D^3}{A d_p}\right)\right] \quad (13)$$

whereas for the capillary force, it will be:

$$\frac{\Delta f}{f_f} = \frac{-\omega m_S}{\pi Z_q} K_A \frac{A_C}{A_0^2}\left[N_M + (N_S - N_M)\Big/\left(1 - \frac{2\omega^2 m_S r}{\pi d_p \gamma_L \cos\theta}\right)\right] \quad (14)$$

## Experimental Section

The diagram of the experimental setup is shown in Figure 1. The 5 MHz AT-cut quartz crystals with 2.54 cm of diameter and 0.33 mm of thickness were supplied by SRS Inc. (Sunnyvale, CA).

(26) Israelachvili, J. N. *Intermolecular and Surface Forces*, 2nd ed.; Academic Press: New York, 1992.
(27) Bocquet, L.; Charlaix, E.; Restagno, F. *C. R. Phys.* **2002**, *3*, 207.
(28) Duran, J.; Jullien, R. *Phys. Rev. Lett.* **1998**, *80*, 3547.
(29) Halsey, T. C.; Levine, A. J. *Phys. Rev. Lett.* **1998**, *80*, 3141.
(30) Hornbaker, D. J.; Albert, R.; Albert, I.; Barabási, A. L.; Schiffer, P. *Nature (London)* **1997**, *387*, 765.

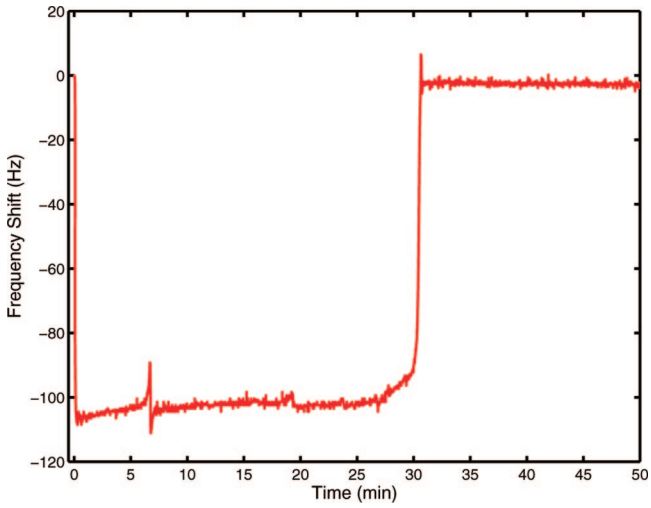


**Figure 2.** The evaporation of a 2 $\mu$L droplet of 50 nm sized alumina particle suspension with a solid concentration of 0.1% w/w on the quartz crystal.

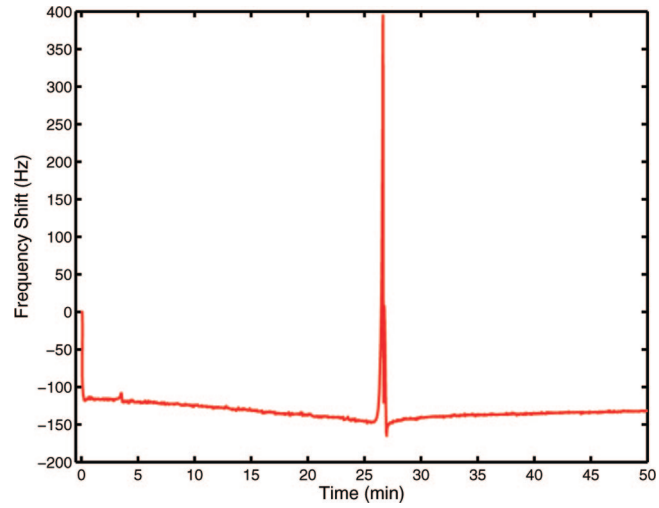


**Figure 3.** The evaporation of a 2 $\mu$L droplet of 50 nm sized alumina particle suspension with a solid concentration of 0.5% w/w on the quartz crystal.

Polished gold electrodes (~160 nm) were deposited on the chromium adhesion layers (~15 nm) on both sides. An asymmetric pattern was used, where the upper electrode in contact with the liquid had a larger radius ($r_{e,upper}$ = 6.45 mm) than the lower one ($r_{e,lower}$ = 3.3 mm). The crystal chip mounted in the standard holder was driven by the RQCM (Maxtek Inc., Santa Fe Springs, CA). Commercially available alumina particles with diameters of 50 nm, 300 nm, and 1 $\mu$m (Sigma-Aldrich, Singapore) were used. The particles were dispersed in 18 MΩ water with varying concentrations. The suspensions were well mixed before extraction, and the droplet was pipetted at the center of the gold electrode. A microscope with homemade crosshair reticule was used to help center the droplet. The droplet volume was 2.0 ± 0.01 $\mu$L, and the initial contact radius of the droplet was about 1.59 mm. The use of the microliter droplets deposited centrally minimized the influence of the Gaussian radial sensitivity distribution and also avoided the generation of compression wave resonance.[3] The droplet was left to evaporate in a glass chamber under our laboratory condition: the temperature was 23 ± 0.5 °C, and the relative humidity was 60 ± 5%. Changes in the resonant frequency during the evaporation were recorded in real-time with the RQCM operating at the fundamental mode. All of the experimental data were processed by a personal computer. The microscope was used with the acoustic measurements, and this allowed observations of the changes in droplet shape. Images of the alumina residue left on the electrode after drying were taken with the microscope. Used crystals were throughout washed in 18 MΩ water followed by ethanol and dried in air for at least 1 h. Each solution was tested at least 10 times. Figures 2–4a are representative curves of crystal response extracted from the repeated trials.

## Results and Discussion

Figure 2 shows the time-dependent frequency shift of the QCM due to the evaporation of the 0.1% alumina suspension droplet of 50 nm sized particles. At $t \approx 0$ min, the deposition of the suspension droplet caused the frequency to decrease ($\Delta f$ = −105.8 Hz) due to the replacement of part of the crystal−air interface with a crystal−liquid interface. Whereas the water evaporation reduced mass detected by the QCM, the sedimentation of the alumina particles caused an inverse effect. The 0.1% suspension of 50 nm sized particles was so dilute that the effect of the water evaporation outweighed that of the alumina particle settling at interface. So the frequency gradually increased due to the mass reduction on the electrode until water was exhausted. The depletion of water was characterized by the sharp peak in frequency shift at $t \approx 30$ min postinjection (Figure 2). The alumina residue left behind the electrode induced a negative frequency shift (ca. −4 Hz). The added mass can be calculated from the resonant frequency shift through the Sauerbrey equation:[31]

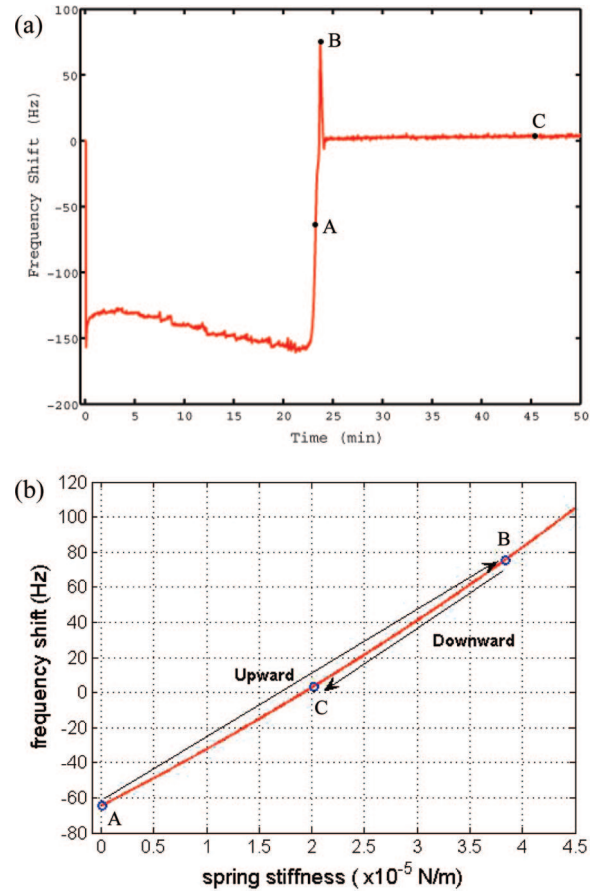


**Figure 4.** (a) The evaporation of a 2 $\mu$L droplet of 50 nm sized alumina particle suspension with a solid concentration of 0.7% w/w on the quartz crystal. (b) Solid line is the calculated dependency of the frequency shift on the effective spring stiffness. Points A−C in both graphics denote the sequential points of interest: (A) at $t \approx 23$ min, it started to account for the contribution of the contact stiffness $k_S$; (B) at $t \approx 24$ min, the maximum peak in frequency shift was measured; (C) the steady frequency shift was measured at $t \approx 45$ min postinjection.

(31) Sauerbrey, G. *Z. Phys.* **1959**, *155*, 206–222.

$$\Delta m = \frac{C}{n}\Delta f \tag{15}$$

where $\Delta m$ is the mass change, $C$ is the mass sensitivity constant ($C = -17.7$ ng/cm$^2$ Hz for a 5 MHz crystal), $n$ is the overtone number ($n = 1, 3, 5...$), and $\Delta f$ is the frequency shift. However, it is found that the Sauerbrey mass predicted by eq 15 is about 30 times smaller than the actual amount of alumina powder in the droplet. The underestimated mass could be due to small contact areas between the alumina particles and the electrode, which transported little stress and induced much less frequency shift of the QCM.[18,25]

Figure 3 shows the time-dependent frequency shift of the QCM due to the evaporation of the 0.5% alumina suspension droplet of 50 nm sized particles. At $t \approx 0$ min, the deposition of the suspension droplet induced the frequency to decrease ($\Delta f = -116.3$ Hz), which was slightly different from the 0.1% suspension droplet. It could be ascribed to the increased density-viscosity product of the suspension droplet with more particles.[32] Thereby the initial frequency shift resulting from the placement of the droplet at the crystal would decrease with the solid concentration. For the 50 nm sized alumina particles, the particle settling at interface outweighed the water loss. Thus, the resonant frequency decreased due to the mass accumulation until water was exhausted by evaporation. The depletion of water was again characterized by the sharp peak at $t \approx 26$ min postinjection, followed by reaching the plateau (ca. $-130$ Hz) at $t \approx 28$ min postinjection. The actual amount of the alumina particles in the droplet was approximately 4 times smaller than the Sauerbrey mass. It suggests that the increased quantities of alumina residue on the electrode could cause an increased number of contacts between the particles and the QCM surface and hence enhance the stress transmission at interface.

Figure 4a shows the time-dependent frequency shift of the QCM due to the evaporation of the 0.7% alumina suspension droplet of 50 nm sized particles. Similar to Figure 3, the influence of the 50 nm sized alumina particles settling at interface outweighed the water loss. The resonant frequency decreased due to the mass sedimentation until water was exhausted by evaporation. The depletion of water was again characterized by the sharp peak at $t \approx 24$ min postinjection, followed by reaching the positive plateau (ca. 6 Hz) at $t \approx 25$ min postinjection. It is interesting to find the positive frequency shift because it is opposed to the Sauerbrey principle (eq 15) that the resonant frequency will decrease with mass added on the crystal surface. A possible mechanism is that after the droplet was dried, clusters of alumina particles were left on the electrode shown as the microscope image (Figure 5a). Inertia held the clusters in place, and the contact stiffness between them was detected by the QCM. As the effect of the contact stiffness outweighed the mass loading, a positive frequency shift was expected. The mass of the alumina particles can be deduced with the known values of the droplet density ($\sim 10^3$ kg/m$^3$), volume ($\sim 2\ \mu$L), and solid concentration ($\sim 0.7\%$), and when divided by the mass of a single particle it yielded the number of the particles $N_S$ ($\sim 5.39 \times 10^{10}$). The contact area $A_C$ ($\sim 7.94$ mm$^2$) can be obtained by imaging the residual spot with the microscope. Dividing $A_C$ by the cross-section area of a single particle ($=\pi d_p^2/4 \approx 1.96 \times 10^{-15}$ m$^2$), it yields $N_M$ ($\sim 4.05 \times 10^9$). Using these values, eq 12 can be used to estimate the effective contact stiffness $k_S$. The solid line in Figure 4b shows the dependency of the frequency shift on $k_S$. Points A−C in Figure 4 represent the time instances of interest:

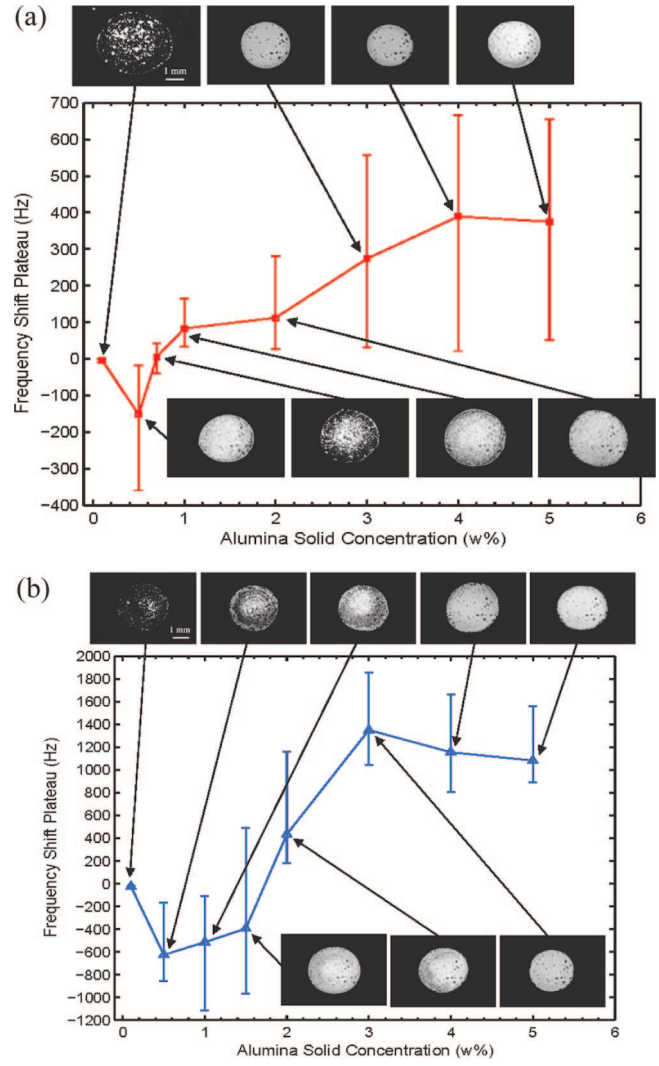


**Figure 5.** Frequency shift upon the residue after completely drying (a) 50 nm (■) and (b) 1 $\mu$m (▲) alumina colloid suspension droplets with varying solid concentration. Representative microscope images taken after the water has evaporated show the residual alumina topography at each concentration.

(A) at $t \approx 23$ min, it started to account for the contribution of the contact stiffness $k_S$; (B) at $t \approx 24$ min, the maximum peak in frequency shift was measured; (C) the steady frequency shift was measured at $t \approx 45$ min postinjection. As shown in Figure 4b, it is clear that the frequency shift becomes positive as the contact stiffness increases.

The frequency responses on the evaporation of the alumina suspension drops of 50 nm sized particles were stabilized within 50 min in all trials. Plotting of the plateau values of the frequency shift versus the 50 nm sized alumina concentration is shown in Figure 5a. Representative microscope images taken after the water has evaporated have shown the residual 50 nm alumina topography at each concentration. The measurements under the same condition were repeated at least 10 times. The spread in the frequency shift after completely drying could be ascribed to the uneven sedimentation of the alumina particles (i.e., the particles did not show uniform distribution and packing configuration) because the spread is not observed when the droplet is first applied to the crystal surface as reflected by the initial frequency shift being less scattering. Furthermore, the influence of spread in particle size and surface roughness of particles might also be taken account for the experimental errors. It is expected that all alumina particles can be rigidly attached to the electrode

(32) Brenner, H. In *Advances in Chemical Engineering*; Drew, T. B., Hoopes, J. W. Jr., Vermuelem, T., Eds.; Academic Press: New York, 1966; Vol. *6*, p 287.

if its quantity is less than a monolayer. It resulted in the negative frequency change whose magnitude increased with concentration. On the other hand, as the quantity of alumina increases beyond the monolayer, a multilayer will be formed. Consequently, the interactions between particles would affect the frequency response. The effect of the contact stiffness was more significant with increased concentration, where larger positive frequency shift was observed. Using the above-mentioned procedure, the effective contact stiffness $k_S$ for 50 nm sized alumina particles at all concentrations (0.7−5% w/w) can be estimated by eq 12 to be around $2 \times 10^{-5}$ N/m.

Two possible mechanisms are examined to verify the sources of the contact stiffness. First, it is hypothesized that the van der Waals force between particles could be a cause of the measured contact stiffness. Using the average estimation of $k_S$ ($\sim 2 \times 10^{-5}$ N/m for 50 nm sized alumina particles) and taking $A = 10^{-19}$ J as a typical value, we can use eq 9 to estimate the distance between the 50 nm sized alumina particles: $D \approx 27.5$ nm. Such magnitude is rational as compared to the particle size. Second, it is hypothesized that the residual water being trapped within the interparticle space can develop liquid bridges around the contact sites between particles, which pull the particles together and increase the contact stiffness. An increased cohesion due to the capillary force known as the sandcastle effect has been well studied.[27–30] Knowing the value of $k_S$, we use eq 11 to estimate the curvature radius of the liquid meniscus: $r \approx 50$ $\mu$m. It is unreasonable that its magnitude considerably exceeds the particle size. Thus, we conclude that for 50 nm alumina particles the contact stiffness cannot be attributed to the capillary force. Instead, it is more likely a result of the van der Waals forces between particles.

The evaporation processes of the alumina suspension droplets with larger particle diameter of 1 $\mu$m on the electrode of the QCM were also studied with varying solid concentrations. Plotting of the plateau frequency shift versus the 1 $\mu$m sized alumina concentration is shown in Figure 5b. The topographies of the residual 1 $\mu$m alumina at each concentration have also been shown by the representative microscope images taken after the water has been evaporated. There are some qualitative differences in the responses between 50 nm and 1 $\mu$m particles. For 1 $\mu$m sized particles, the positive frequency shift was also found as the alumina concentration increased beyond 1%. Yet the effective contact stiffness for all concentrations (1−5% w/w) was around $3 \pm 1$ N/m, which is $10^5$ times larger than 50 nm sized particles. Similarly, the source of the contact stiffness for 1 $\mu$m particles was also verified. For the van der Waals force, using the average value of $k_S$ ($\sim 3$ N/m) and taking $A = 10^{-19}$ J, the distance between 1 $\mu$m sized alumina particles can be estimated: $D \approx 1.4$ nm, unreasonable as compared to the particle size. On the other hand, for the capillary force, the radius of curvature of the liquid meniscus is estimated to be $r \approx 6.6$ nm, which is well consistent with the earlier studies. Therefore, we conclude that, for 1 $\mu$m sized alumina particles, the measured contact stiffness is likely caused by the capillary force rather than the van der Waals force. Moreover, it is found in Figure 5b that the magnitudes of the frequency increment tend toward saturation at high concentrations, implying that the effective contact stiffness deduces with increased solid concentration. Similar behavior is observed for 300 nm sized alumina particles (Figure 6). One possible explanation is that the water condensation around the contact sites between the larger particles should be dependent on the particle size and packing configuration. However, the quantitative analysis of the capillary force on each condition is not available yet. In summary, the present work is related to the application of alumina powder for ceramic tool sintering.[21] QCM appears to be an accurate and attractive method for determining the amount of alumina powder required for the colloidal suspension. However, the present work has shown that the results from QCM measurements are highly dependent on the particle size and the interparticle interactions and must be used with caution.

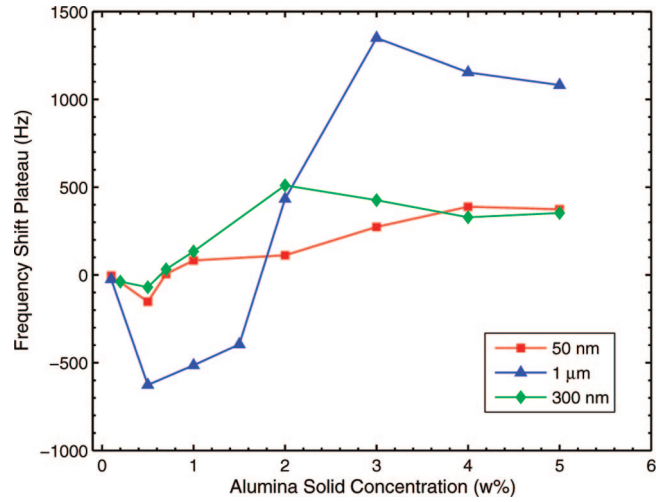


**Figure 6.** Frequency shift versus solid concentration after completely drying alumina colloidal suspension droplets with different particle sizes: (□) 50 nm; (▲) 1 $\mu$m; (♦) 300 nm. Standard error bars have been omitted for clarity.

## Conclusion

In this Article, we have reported the application of the QCM for the study of the evaporation of colloidal suspension droplets on the QCM surface. Droplets of alumina particle suspensions with varying particle size and solid concentration were studied. Characteristic responses of the crystal resonant frequency, associated with the different evaporation stages, were found, and the results showed the dependency on the particle size. Quantitative analysis of the experimental data was performed by using the QCM models proposed in this Article. While the mass interpretation can be applied to describe the adsorption of the alumina particles from the dilute suspensions, for the concentrated suspensions it needs to account for the effects of the contact stiffness on the frequency responses. More importantly, positive frequency changes after the complete evaporation were observed for some suspensions. Interpretation of the positive frequency changes in term of the contact stiffness was developed. Possible physical mechanisms for the contact stiffness were also discussed and quantified in terms of the interparticle forces including the van der Waal force and capillary force. It has been found that, whereas for the small particles the van der Waal force was responsible to the contact stiffness, for the larger particles the capillary force arising from the sandcastle effect dominated. However, the quantitative account of the capillary force at each concentration will be discussed in future work. The present study on the sedimentation of alumina powders is related to the development of nanomaterials and ultrathin functional coatings of nanoparticles. QCM appears to be an accurate and attractive method for determining the amount of alumina powder required for the colloidal suspension. However, the present work shows that the results from QCM measurements are highly dependent on the particle size and the interparticle interactions and must be used with caution.

LA800661G